Results in Engineering 30 (2026) 109795

Contents lists available at ScienceDirect

Results in Engineering

journal homepage: www.sciencedirect.com/journal/results-in-engineering

Research paper

Effect of flexibility degree in tubular joints on continuous genetic algorithm-based optimization of offshore jacket-type platforms

Naser Shabakhty [*], Hamid Reza Karimi, Abbas Yeganeh-Bakhtiay, Mohammad Ghanbarian

School of Civil Engineering, Iran University of Science and Technology (IUST), Tehran, Iran

ARTICLE INFO

Keywords:
Offshore jacket platforms
Genetic algorithm optimization
Joint flexibility
Elastic-plastic behavior
Efficiency

ABSTRACT

The optimization of offshore jacket platforms remains a critical challenge in marine engineering, requiring a balance between structural integrity, material efficiency, and cost. This study develops a continuous genetic algorithm (CGA) framework that explicitly integrates joint flexibility and codified design criteria. Four scenarios were evaluated: rigid joints, flexible joints with MSL criteria, flexible joints with API RP 2A criteria, and fixed-brace optimization. The rigid-joint model achieved a 31% weight reduction (1,437→996 tons), while incorporating joint flexibility improved outcomes: the MSL-based flexible model achieved 34% (943 tons), and the API-based flexible model achieved the highest reduction at 35% (934 tons). These improvements were accompanied by increases in the fundamental period (1.02→1.91 s) and deflection (65.7→156.4 mm), indicating realistic stress redistribution through elastic–plastic joint behavior. In contrast, the fixed-brace model yielded only 19% savings (1,170 tons) due to restricted load paths. Convergence analysis showed stable optimization within 90–100 generations, highlighting the robustness of the CGA. Sectional results revealed that jacket legs contributed up to 42% of the optimization in constrained scenarios, while simultaneous brace–leg optimization enabled holistic weight reduction. Overall, the proposed flexibility-aware framework achieves 30–35% material savings compared with traditional rigid models, without violating API displacement and stress constraints, thereby demonstrating its value for cost-effective and safe design.

1. Introduction

Offshore jacket structures are pivotal in supporting and stabilising various marine installations, including oil and gas platforms, wind turbines, and other maritime infrastructures. These structures typically comprise tubular joints and steel members arranged in a framework that distributes the loads imposed by environmental forces [1–3]. The design and optimization of offshore jackets are critical to ensure their structural integrity, longevity, and economic viability. As the offshore industry expands into deeper and more challenging environments, the demand for efficient and robust optimization methods for jacket configurations has become increasingly significant [4–6].

The complexity inherent in offshore jacket design arises from many factors that must be simultaneously considered to achieve an optimal configuration. These factors encompass structural performance criteria, material costs, construction feasibility, maintenance requirements, and environmental impact. Additionally, the flexibility degrees of tubular joints, which refer to the range of movements allowed at the connections between structural members, add another layer of complexity to the optimization process [7–9].

The flexibility of these joints influences the overall behavior of the structure under various loading conditions, affecting its dynamic response and static stability. Considering the different flexibility degrees of tubular joints introduces a critical dimension to optimizing offshore jacket configurations. Flexible joints can accommodate movements caused by environmental loading, thereby reducing stress concentrations and enhancing the overall resilience of the structure. However, excessive flexibility may lead to undesirable deformations and affect the platform's operational stability. Conversely, overly rigid joints may increase the structural mass and material costs while potentially exacerbating stress distributions [10–12]. In practical offshore engineering, the distinction between rigid and flexible joint modeling has direct implications for both safety and cost. Rigid-joint assumptions artificially increase global stiffness, leading to shorter natural periods, reduced lateral drift, and consequently larger member sizes to satisfy stress and buckling constraints. When realistic joint flexibility is introduced (using MSL or API RP 2A capacity models), the structure exhibits a more accurate elastic–plastic rotation at tubular connections. This reduces the jacket's

* Corresponding author.
E-mail address: shabakhty@iust.ac.ir (N. Shabakhty).

https://doi.org/10.1016/j.rineng.2026.109795
Received 3 August 2025; Received in revised form 8 February 2026; Accepted 26 February 2026
Available online 26 February 2026

effective stiffness, increases the natural period and deck displacement, and redistributes forces among the legs and braces. As a result, the optimization algorithm avoids unnecessary overdesign and identifies lighter yet code-compliant configurations.

Traditional optimization approaches in offshore jacket design often rely on deterministic methods such as linear programming, nonlinear programming, and gradient-based techniques. While these methods can be effective for problems with well-defined parameters and objectives, they often fail to address the inherent uncertainties associated with offshore environments [13]. Moreover, the discrete nature of conventional optimization techniques may limit their ability to explore the vast and complex design space effectively. Consequently, there is a growing interest in leveraging evolutionary algorithms, particularly genetic algorithms (GAs), to overcome these limitations and achieve more comprehensive and adaptable optimization solutions [14–16].

Genetic algorithms (GAs), inspired by natural selection and genetics, are evolutionary techniques for complex optimization with multiple objectives and large search spaces. Unlike traditional methods, GAs use a population that evolves through selection, crossover, and mutation, exploring diverse solutions and avoiding local optima. Continuous GAs (CGAs) extend this to continuous variables, improving efficiency. In offshore jacket design, CGAs fine-tune parameters like member lengths and angles, exploring the design space more thoroughly. When integrated with optimization frameworks, CGAs can find Pareto-optimal solutions, balancing multiple objectives [17–20]. Recent advances in computational optimization show hybrid approaches, combining algorithms like CGAs with structural analysis, are effective for offshore jacket design. These methods improve structural stiffness, response, material use, and cost, supporting sustainable offshore wind farms. Using genetic algorithms can reduce materials and costs while improving performance and adaptability.

1.1. Literature review

Several studies have explored the use of genetic algorithms in optimizing offshore structures, demonstrating their capability to generate high-quality solutions that meet diverse design objectives. However, integrating joint flexibility considerations into these optimization frameworks remains underexplored. Most existing research focuses on optimizing structural geometry and member sizing without adequately addressing the pivotal role of joint behavior. This gap underscores the need for comprehensive optimization approaches that encompass geometric configurations and joint connections' mechanical properties.

Gentils et al. [21] investigate the structural optimization of offshore wind turbine (OWT) support structures using a combination of Finite Element Analysis (FEA) and Genetic Algorithm (GA). Given that support structures account for nearly 25% of the total capital cost of an OWT, their optimization plays a crucial role in reducing the overall cost of offshore wind energy. The optimization process involves selecting the outer diameters and section thicknesses as design variables while incorporating constraints such as vibration, stress, deformation, buckling, fatigue, and standard design criteria.

Benítez-Suárez et al. [22] explore the use of Particle Swarm Optimization (PSO) to design and optimize jacket substructures for offshore wind turbines. Results show that the use of precomputed initial swarms, based on a concept design with low computational cost, significantly enhances the efficiency and effectiveness of the PSO algorithm compared to standard random populations. A case study using the NREL-5 MW wind turbine and its OC4 reference jacket substructure illustrates the capabilities of the proposed methodology.

Ivanhoe et al. [23] develop a generic framework for the reliability assessment of offshore wind turbine (OWT) jacket support structures under stochastic and time-dependent variables. OWTs are subjected to harsh marine environments, where uncertainties in environmental loads and soil properties pose challenges in assessing structural integrity. The authors present a non-intrusive reliability assessment framework that integrates parametric finite element analysis (FEA) and multivariate regression to evaluate structural performance under varying input conditions. The framework considers five key limit states (buckling, deflection, fatigue, frequency, and ultimate limit states). Reliability indices for these limit states are computed using the First Order Reliability Method (FORM) to estimate low probability failure values. The methodology is applied to the NREL 5 MW OWT OC4 jacket, demonstrating that the structural components of the jacket exhibit acceptable reliability levels under stochastic conditions.

Lee et al. [24] investigate the structural topology optimization of the transition piece in an offshore wind turbine with a jacket foundation. The authors compare conventional trial-and-error heuristic design approaches with topology optimization techniques to improve structural performance. A 5 MW reference wind turbine with jacket support is used as a case study, where a topology-optimized transition piece is developed alongside a traditionally designed counterpart. Verification results indicate that the topology-optimized design is lighter and exhibits reduced stress concentrations, which significantly enhances its fatigue life.

Wang et al. [25] present a numerical tool for efficiently analyzing and optimizing offshore wind turbine jacket substructures. Two optimization methods were explored to optimize the jacket substructure: parametric optimization and genetic algorithm (GA) optimization. Results show that parametric optimization achieves mass reductions of 6.2%, 10%, and 14.8%, while GA optimization is more aggressive, achieving reductions of 16.8%, 22.3%, and 34.3% but at a higher computational cost.

As the literature review shows, previous studies on GA-based optimization of offshore jackets have primarily treated tubular joints as rigid or applied highly simplified connection models, thereby overlooking the influence of local joint flexibility on global response and design efficiency. This assumption can lead to either over-conservative or unsafe designs, since joint flexibility affects lateral drift, natural period, and stress distribution.

1.2. Aims and scope

The present study aims to bridge this gap by developing a continuous genetic algorithm-based optimization framework tailored for offshore jacket configurations. This framework explicitly incorporates the varying flexibility degrees of tubular joints, enabling a more holistic optimization process that accounts for both structural performance and material efficiency. By doing so, the proposed methodology aspires to deliver optimized jacket designs that are cost-effective, resilient, and adaptable to the dynamic marine environment.

To achieve this, the study first formulates the offshore jacket optimization problem as a model, delineating the key performance metrics such as structural stiffness, dynamic response characteristics, material usage, and construction costs. The flexibility degrees of tubular joints are parametrized and integrated into the optimization variables, allowing the genetic algorithm to explore joint configurations alongside the overall jacket geometry. The continuous nature of the genetic algorithm facilitates the precise adjustment of these parameters, ensuring that the optimization process can attain finely tuned solutions.

Subsequently, the proposed continuous genetic algorithm is deployed to explore the design space, leveraging its evolutionary operators to enhance the population of candidate solutions iteratively. The algorithm evaluates each candidate jacket configuration against the defined objectives, employing fitness functions that quantify performance metrics and guide the selection process toward optimal tradeoffs. The Pareto front generated by the algorithm provides a spectrum of optimal solutions, each representing a different balance among the competing objectives, thereby offering valuable insights for decision-makers in the design process.

The novelty of the present study lies in explicitly incorporating joint flexibility—using both MSL and API RP 2A joint capacity models—directly into the GA optimization process. This integrated framework allows for a more realistic evaluation of serviceability and strength constraints, ensuring that the optimized jackets not only minimize weight but also remain safe and code-compliant under true joint behavior.

2. Genetic algorithm and optimization

2.1. Genetic algorithm

Genetic algorithms (GAs), inspired by the processes of natural evolution, are a type of machine learning model. They fall under optimization algorithms designed to identify global or nearly optimal solutions. GAs generate a population of individuals, each represented as a chromosome with a specific structure, which proposes possible solutions to a given problem. These chromosomes are assessed against the optimization criteria, with those yielding superior solutions being more likely chosen as parents for the next generation. The evolution process then occurs among the individuals within the population. In practical applications, a computational genetic model is implemented using arrays of bits or characters representing chromosomes, enabling crossover and mutation operations by manipulating these bits or strings. Generally, the initial generation is formed randomly. Every individual in the population undergoes evaluation, and the subsequent generation is developed by employing selection, crossover, and mutation operations on the existing population. This evolutionary cycle continues until the desired optimal solution is achieved, optimizing the objective function. Essentially, GAs are search and optimization methods rooted in genetic principles and natural selection, leading a population of individuals toward a peak fitness state across successive generations, effectively minimising the cost function. Although primarily known for function optimization, the scope of GAs extends beyond this application. Introduced by John Henry Holland in 1975, GAs have grown to include any population-based model that utilizes selection and combination operators to generate new samples in a search space. Continuous genetic algorithms directly handle continuous variables to minimize costs. In contrast, discrete GAs require many bits representing each variable, resulting in longer chromosomes when many variables are involved. While binary representation is prevalent, various methods can encode variables. Discrete GAs excel with naturally quantized variables, but representing continuous ones as floating-point numbers is more practical. Their discrete representation constrains the precision of discrete GAs, whereas continuous GAs can achieve full precision using real numbers. Continuous GAs offer lower storage demands, using a single actual number to represent a variable rather than multiple bits. They typically operate faster than discrete GAs since variable decoding is unnecessary when evaluating the cost function. Differences in variable representation between continuous and discrete GAs also lead to distinct crossover and mutation techniques. Continuous GAs are generally favored because they eliminate the need for binary conversions and bit assignments related to variables. They also integrate more seamlessly with other optimization algorithms, making collaboration easier. GAs consist of several components and operators, including chromosome structure, evaluation function, population, method for parent selection, crossover and mutation operators, and replacement strategy. To optimize a problem with GAs effectively, it is essential to define these components, operators, the termination conditions for the algorithm, and the approach for establishing the initial population [26,27].

In GAs, a chromosome represents a potential solution to the problem at hand. It's typically encoded as a string of genes, which can be binary digits, real numbers, or other data types, depending on the specific implementation and problem domain. Each gene within the chromosome signifies a particular aspect of the solution. A population is a collection of chromosomes present in a given generation. The size of the population can influence the algorithm's performance, affecting both the diversity of solutions and the computational resources required. A diverse population helps in exploring a broader search space, increasing the chances of finding an optimal or near-optimal solution. Selection is the process of choosing chromosomes from the current population to act as parents for the next generation. This process is typically guided by a fitness function, which evaluates how well each chromosome solves the problem. Chromosomes with higher fitness scores have a greater probability of being selected, promoting the propagation of advantageous traits. Mating, or crossover, is a genetic operator that combines two parent chromosomes to produce offspring for the next generation. This process involves exchanging segments of the parent chromosomes, allowing the offspring to inherit traits from both parents. Crossover promotes the exploration of new solutions by recombining existing genetic material. Mutation introduces random alterations to individual genes within a chromosome. This operator ensures genetic diversity within the population, preventing premature convergence to suboptimal solutions. By exploring new areas of the solution space, mutation helps maintain the algorithm's robustness and adaptability. Insertion, also known as reinsertion, is the process of integrating offspring back into the population, replacing some of the existing chromosomes. This step ensures that the population size remains constant across generations. Strategies for insertion can vary; some approaches replace the least fit individuals, while others use more sophisticated methods to maintain diversity and prevent the loss of valuable genetic material. Stopping criteria determine when the genetic algorithm should terminate. Common stopping conditions include reaching a predefined number of generations, achieving a satisfactory fitness level, or observing no significant improvement over several generations. Appropriate stopping criteria are crucial to balance solution quality and computational efficiency [28,29].

2.2. Optimization

The optimization process was conducted using four models. In Model-1 the connections between members were modeled as rigid joints based on traditional methods. The optimization process was applied to all elements of the jacket structure, and the model analysis was linear. In Model-2, the flexibility of the connections was modeled using nonlinear relationships provided by MSL. In this model, instead of considering the connection as a dimensionless point where members are rigidly connected, it was modeled as a structural member. Model-3 is similar to Model-2, with the difference that the connection capacity relationships used for the nonlinear MSL relationships are those provided by the API RP 2A code. Model-4 was also similar to Model-2, but optimization was performed only on the jacket's legs. Table 1 shows the details of each model.

In all four models, loading conditions were identical, considering extreme storm conditions with a 100-year return period and maximum seawater depth up to the seabed level. Platform members were subjected to dead and live weight loads and environmental loads from waves, currents, and wind. Wave forces were significantly higher than environmental forces acting on the platform. Design responses were analyzed for pre-operational conditions, including fabrication onshore, loading onto the transport barge, transfer to the installation site, lifting with a crane, and post-operational conditions, such as vessel collision, earthquake occurrence, and marine corrosion. The optimized structural members had approximately 95 cross-sections, with diameters ranging from 4.5 to 120 inches and thicknesses between 2 and 65 millimeters. Therefore, considering the discrete nature of the decision variables, the optimization problem was formulated as a discrete optimization problem.

The objective function or fitness function is to minimize the total weight of the platform. The weight of each structural member is calculated by multiplying the cross-sectional area of the members by their density and length, which are constant values for each member. The total weight of the jacket is equal to the sum of the weight of the jacket structure and the weight of the upper deck structure of the platform.

Table 1
The details of each model considered for the optimization process.

	Model-1	Model-2	Model-3	Model-4
Groups Optimized	All groups	All groups	All groups	L1, L2, and L3
Joint Modeling	Rigid	Flexible with MSL joint capacity	Flexible with API joint capacity	Flexible with MSL joint capacity
Selection Method	**stochastic** uniform sampling with tournament size of 2			
Elite Chromosomes per Generation	2 chromosomes			
Mutation probability	0.05 (Gaussian mutation, scale = 1, shrink = 1)			
Seeding	Random initialization with MATLAB default random seed (rng default), repeated runs performed with rng seeds 1–20 for robustness			
Crossover probability	0.8 (intermediate crossover)			
Replacement Method	Complete replacement			
Population Size per Generation	50 chromosomes			
Stopping Condition	No improvement in the best fitness for 20 consecutive generations, or a maximum of 150 generations			

Since the optimization process only affects the jacket structure, the weight of the jacket structure changes during the process, while the weight of the upper deck structure remains constant. The total weight of the platform is given by the Eq. (1). Where the weight of the jacket structure is calculated using Eq. (2)

$$W_{\text{total}} = W_{\text{Jacket Structure}} + W_{\text{Deck Structure}} \tag{1}$$

$$W_{\text{Jacket Structure}} = \sum_{E=1}^{i} L_E A_E \rho \tag{2}$$

In this equations L_i is the length of the jacket structural members (in meters). A_i is the cross-sectional area of the jacket structural members (in square meters), and ρ is the unit weight of the jacket structure members, which is a constant value of 7849 Kg/m^3.

This study applies a penalty to invalid solutions during the optimization process. The cost function of the genetic algorithm is modified by adding an external penalty function to the objective function, which is the platform's weight. Specifically, the penalty is applied to invalid solutions, effectively transforming the constrained optimization problem into an unconstrained one by eliminating invalid solutions due to the high cost resulting from penalties. During the optimization process, any design or solution that has a maximum stress ratio, maximum horizontal displacement ratio, or shear stress ratio greater than 1 is considered invalid and penalized. This penalty increases the cost of invalid designs, reducing their fitness for the next generation. The penalized fitness function is given by the Eq. (3),

$$W = W_{\text{Jacket Structure}} + W_{\text{Jacket Structure}} \cdot \sum_{n=1}^{nc} [\max(0, B_n - 1]^2$$

$$B_n = V_n^{actual} / V_n^{allowable} \tag{3}$$

where V_n^{actual} is the measured value for constraint n (e.g., maximum axial stress, horizontal displacement at reference point, shear at connection, slenderness ratio, etc.) and $V_n^{allowable}$ is the allowable value for that same constraint, and a value $B_n>1$ indicates a violation. The penalized fitness used by the GA is Eq. (4).

$$F(x) = W(x) + P(x) \tag{4}$$

with the penalty P chosen from two options, a static quadratic penalty (Eq. (5)) and a dynamic penalty (Eq. (6)).

$$P_{static}(x) = C \sum_{n=1}^{N_c} [\max(0, B_n(x) - 1)]^p \tag{5}$$

$$P_{dyn}(x, g) = C_0 \left(1 + \frac{g}{G_{max}}\right)^{\kappa} \sum_{n=1}^{N_c} [\max(0, B_n(x) - 1)]^p \tag{6}$$

Where g is the generation index, G_{max} is the maximum allowed generations, and C, C_0, p, κ are penalty constants. In the current paper, a dynamic schedule is used by default with C_0=100, κ=3, p= 2, and G_{max}=150. The ratio B_n and penalty were computed for each constraint (stress, displacement, buckling, shear, punching), and violation statistics were recorded per generation across 20 independent runs (seeds 1–20).

It should be noted that applying external penalties converts the constrained optimization into a penalized single-objective formulation: infeasible designs remain searchable but are assigned a larger (worse) fitness. This does not algebraically remove constraints; it enforces them numerically by discouraging violations.

The optimization constraints encompass design limits on stress, buckling, connection shear, and displacement. Stress constraints address axial, shear, in-plane bending, and out-of-plane bending stresses. Shear stresses in connections must not exceed permissible values as specified in the 21st edition of the API RP 2A-WSD standard. The lateral drift limit is defined as $\delta_h \leq H/200$, enforced at the deck reference elevation by defining $H = z_{ref} - z_{mud}$ (the vertical distance from the mudline to the deck-level global response point, the intersection of the jacket centerlines at the deck plane) and the resulted horizontal displacement at the reference point (δ_h). Buckling is evaluated by determining the slenderness ratio for overall buckling and the diameter-to-thickness ratio for local buckling in tubular members, ensuring these ratios do not exceed specified limits. Throughout the optimization, the normalized values of these constraints should not surpass 1 to maintain structural integrity. For comprehensive guidelines on allowable stress design for offshore platforms, refer to the API RP 2A-WSD standard.

To manage the complexity of the optimization problem and reduce the number of decision variables, the jacket's structural members are grouped into leg groups, vertical Brace groups, and horizontal brace groups. In leg groups, each group consists of four members corresponding to the legs between two consecutive deck levels, starting from the seabed. These members have a composite cross-section, with the leg and pile diameters and thicknesses being design variables (the groups are named LG-1, LG-2, and LG-3). Brace groups include diagonal and vertical braces, each containing 16 or 20 members between two consecutive deck levels (the groups are named VB-1, VB-2, and VB-3). In horizontal brace groups, each group consists of horizontal braces at every four deck levels, named HB-1, HB-2, HB-3, and HB-4. The details of member grouping are shown in Fig. 1.

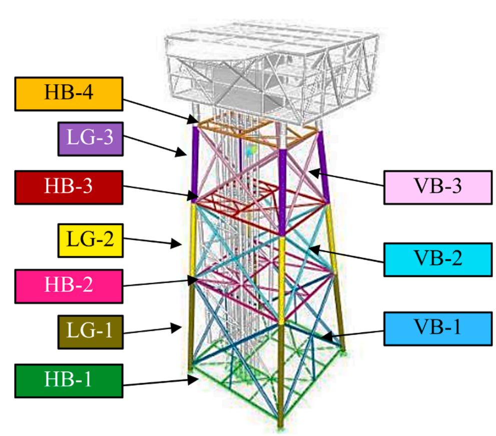

Fig. 1. Schematic view of the offshore jacket-type platform, a) 3-D view, and the grouping IDs.

Table 2 shows the initial diameter and thickness of the platform's members. In the optimization process, the selection of cross-sections and the determination of the diameter and thickness of the tubular sections for each group (gene) are discrete. These are chosen from among 95 predefined cross-sections for structural members, with diameters ranging from 4.5 to 120 inches and thicknesses ranging from 2 to 65 millimeters.

3. Platform modeling and joint flexibility model

3.1. Platform's structure and loading

In the model, the top of the jacket is positioned at an elevation of 7.25 m above LAT, while the jacket walkway frame is located at 5.75 m above LAT. The frames within the jacket structure are positioned at the following elevations: the second frame at 13 m below LAT, the third frame at 35 m below LAT, the conductor guide frame at 61.2 m below LAT, and the fourth frame at the seabed or mud line level at 64.7 m below LAT. The water depth at the platform's location is 64.7 m below LAT, which is also taken as the Chart Datum reference level. Fig. 2 presents views of the platform model created in finite element software.

The platform has a single-battered leg on one side (1:7) and a double-battered leg configuration on the other side (1:7 and 1:8). The dimensions between the legs at the working point elevation are 24 m × 13.72 m. The platform's foundation is comprised of four piles. The structure's natural periods in the initial design and optimized design are 1.28 sec and 2.14 sec, respectively. Since the structure's natural period is less than 3 sec, dynamic amplification factors on wave loads are not included.

4.2. Loads

Loads on the platform were applied in dead, live, and environmental groups. Dead loads are permanent loads on each floor, such as electrical, instrumentation, and mechanical equipment, dry. Live loads are included in the open, lay down, muster, and building areas. Environmental data were based on field data (100-year storm). The corresponding directions of environmental data are shown in Table 3.

The wind force can be calculated using Eq. (7), where ρ_a is the density of air, U_{wind} is the wind speed, C_S is the shape coefficient, and A is the area of the object.

$$F = (\rho_a/2){U_{wind}}^2 C_s A \tag{7}$$

Wave loads are calculated using the Morison equation as outlined in API-RP-2A-WSD. For the wave force and current force per unit length, Morrison's formula is used to calculate the drag force and inertia force, as shown in Eq. (8).

$$F = (\rho/2)C_D A|u_x|u_x + \rho C_M V \dot{u}_x \tag{8}$$

Where A is the projection area per unit length pile column perpendicular to the vector u_x, V is the drainage volume for the unit length of the component. u_x and $\dot{u}_x$ are the relative velocity and acceleration vectors perpendicular to the axial component obtained by Stokes solution. C_M is the inertia force coefficient.

The water depth was 64.7 m below the Lowest Astronomical Tide (LAT). For the in-place analysis, the minimum water depth is taken as LAT, while the maximum still water depth is determined as the sum of LAT, the Mean Higher High Water (MHHW), and the 100-year Storm Surge, as detailed in Table 4.

Finally, the design load combinations are formed based on the 100-year extreme storm conditions and the maximum 100-year static water depth, considering deadweight loads, environmental loads, and 50% of live load weight, which is shown in Table 5.

In accordance with the specified standards, the Unity Check (UC) ratios are computed for all members as per the relevant guidelines. These ratios guarantee that the stresses or buckling experienced by the members remain within permissible limits as defined by the equations outlined in the applicable codes. For members subjected to tension or tension in conjunction with bending, the evaluations are conducted in accordance with the API standards utilising Eq. (9). This process ensures adherence to the design requirements and the structural safety of the platform [30].

$$UC = \frac{f_a}{0.6F_y} + \frac{\sqrt{{f_{bx}}^2 + {f_{by}}^2}}{F_b} \leq 1.0 \quad UC = \frac{f_b}{F_b} \leq 1.0 \tag{9}$$

In Eq. (10), *fa* represents axial stress, *fb* denotes bending stress, *fbx* refers to bending stress about the local x-axis, f_{by} indicates bending stress about the local y-axis, *Fy* signifies yield stress, and *Fb* is the allowable bending stress. For members subjected to compression (where compressive stress is less than or equal to $0.15F_a$, Eq. (10) may be utilised to calculate the ultimate capacity (UC), where *Fa* represents allowable axial compressive stress.

$$UC = \frac{f_a}{F_a} + \frac{\sqrt{{f_{bx}}^2 + {f_{by}}^2}}{F_b} \leq 1.0 \tag{10}$$

Tubular members subjected to combined compression and flexure with compressive stress greater than 0.15*Fa* were also checked using Eq. (11) where *Fe'* is Euler buckling stress per AISC code and *Cm* is the coefficient applied to the bending term in the interaction formula and dependent upon column curvature caused by applied moments [30]:

$$UC = \frac{f_a}{0.6F_y} + \frac{\sqrt{{f_{bx}}^2 + {f_{by}}^2}}{F_b} \leq 1.0 \quad UC = \frac{f_a}{F_a} + \frac{C_m\sqrt{{f_{bx}}^2 + {f_{by}}^2}}{\left(1 - \frac{f_a}{F_e^{'}}\right)F_b} \leq 1.0 \tag{11}$$

The Euler buckling stress ratio for members in compression was determined by Eq. (12).

$$UC = \frac{f_a}{F_e^{'}} \leq 1.0 \tag{12}$$

The shear unity check ratio was also taken as the larger of the Eq. (13) [30].

$$UC = \frac{f_v}{F_v} = \frac{f_v}{0.4F_y} \leq 1.0 \quad UC = \frac{f_{vt}}{F_{vt}} = \frac{f_{vt}}{0.4F_y} \leq 1.0 \tag{13}$$

In Eq. (10), *fv* is shear stress due to shear force, *fvt* is shear stress due to torsion, *Fv* is allowable shear stress, and *Fvt* is allowable torsional shear stress.

To control the connections, the maximum stress ratio should be checked for punch shear according to Eq. (14) [30]:

$$UC = \frac{v_p}{v_{pa}} = \frac{\tau f \, \sin\theta}{Q_q Q_f F_{yc}/0.6\gamma} \leq 1.0 \tag{14}$$

In Eq. (11), *vp* represents the punching shear, and *vpa* is the

Table 2
The initial diameter and thickness of members.

Groupe	Diameter (mm)	Thickness (mm)	Diameter of pile (mm)	Thickness of pile (mm)
L-1	1755	65	1524	44.45
L-2	1755	65	1524	44.45
L-3	1755	65	1524	44.45
VB-1	864	25.4	-	-
VB-2	610	25.4	-	-
VB-3	610	38.1	-	-
HB-1	660	25.4	-	-
HB-2	660	25.4	-	-
HB-3	610	25.4	-	-
HB-4	610	25.4	-	-

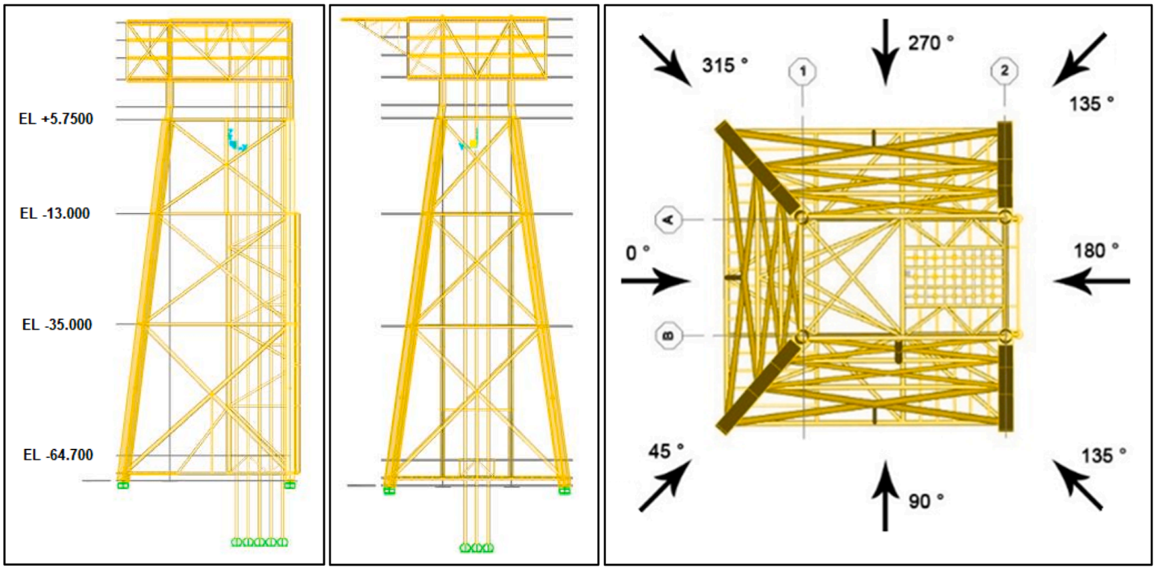

Fig. 2. The platform model in software and eight wave, current, and wind directional headings.

Table 3
Environmental data for 100-year extreme storm conditions.

Geographical Direction	water depth (m)	Wind Velocity (m/s)	Current data (m/s)	Wave data	
				Height (m)	Period (s)
South East (0°)	66.4	35.6	Surface =	9.7	10.0
East (45°)	66.4	34.9	1.28	8.8	9.6
North East (90°)	66.5	36.0	Mid-Depth=1.28	10.8	10.4
North (127°)	66.6	35.2	Seabed=0.71	11.6	10.8
North West (180°)	66.5	33.4		10.2	10.2
West (225°)	66.4	33.0		8.8	9.5
South West (270°)	66.5	35.6		10.8	10.4
South (315°)	66.6	36.7		12.2	11.0

Table 4
100-year maximum still water depth data.

Parameter	Value (m)							
	N	NE	E	SE	S	SW	W	NW
LAT above seabed	64.7	64.7	64.7	64.7	64.7	64.7	64.7	64.7
MHHW above LAT	1.6	1.6	1.6	1.6	1.6	1.6	1.6	1.6
100-year storm surge	0.1	0.1	0.2	0.3	0.2	0.1	0.2	0.3
100-year Total SWL	66.4	66.4	66.5	66.6	66.5	66.4	66.5	66.6

allowable punching shear stress calculated for each component of brace loading and joint type K, X, T, or Y using the *Qq* and *Qf* factors. *Qq* accounts for loading type and geometry effects on the joint, while *Qf* considers the influence of nominal longitudinal stress in the chord member. The nominal stress *f* refers to axial stress, in-plane bending stress, or out-of-plane bending stress in the brace, with punching shear for each member evaluated separately. The yield strength of the chord member at the joint, *Fyc*, is either the yield strength or two-thirds of the tensile strength, whichever is less. The joint geometry parameters θ, τ, and γ are defined in Fig. 3 [30], ensuring that the punching shear capacity aligns with the required structural performance criteria.

Each tubular connection is also evaluated to ensure its ability to carry

Table 5
The load combination details.

Comb-1	Dead load + 50% of live load + environmental loads in extreme storm conditions and maximum depth for a 100-year period in the 0° direction.
Comb-2	Dead load + 50% of live load + environmental loads in extreme storm conditions and maximum depth for a 100-year period in the 45° direction.
Comb-3	Dead load + 50% of live load + environmental loads in extreme storm conditions and maximum depth for a 100-year period in the 90° direction.
Comb-4	Dead load + 50% of live load + environmental loads in extreme storm conditions and maximum depth for a 100-year period in the 135° direction.
Comb-5	Dead load + 50% of live load + environmental loads in extreme storm conditions and maximum depth for a 100-year period in the 180° direction.
Comb-6	Dead load + 50% of live load + environmental loads in extreme storm conditions and maximum depth for a 100-year period in the 225° direction.
Comb-7	Dead load + 50% of live load + environmental loads in extreme storm conditions and maximum depth for a 100-year period in the 270° direction.
Comb-8	Dead load + 50% of live load + environmental loads in extreme storm conditions and maximum depth for a 100-year period in the 315° direction.

at least 50% of the effective strength of the connecting brace. This requirement is considered satisfied for simple tubular joints when Eq. (15) is met, where *Fyb* is the yield strength of the brace member, and θ, τ, γ, and β are joint geometry parameters shown in Fig. 3.

$$UC = \frac{F_{yb}(\gamma\tau\ \sin\theta)}{F_{yc}\left(11 + \frac{1.5}{\beta}\right)} \le 1.0 \tag{15}$$

3.2. Joint flexibility model

In analyzing structures with tubular members, such as offshore jackets, the connections between members are traditionally assumed to be rigid. In fact, the connection is considered a dimensionless point where the members are rigidly connected without modeling it as a structural member. This assumption implies no axial or rotational deformation at the ends of the sub-members relative to the primary member. However, in reality, local deformations occur in the cross-section of the member under the applied loads. This indicates that tubular connections possess significant flexibility within the elastic-plastic range. Consequently, the results of analyses based on the

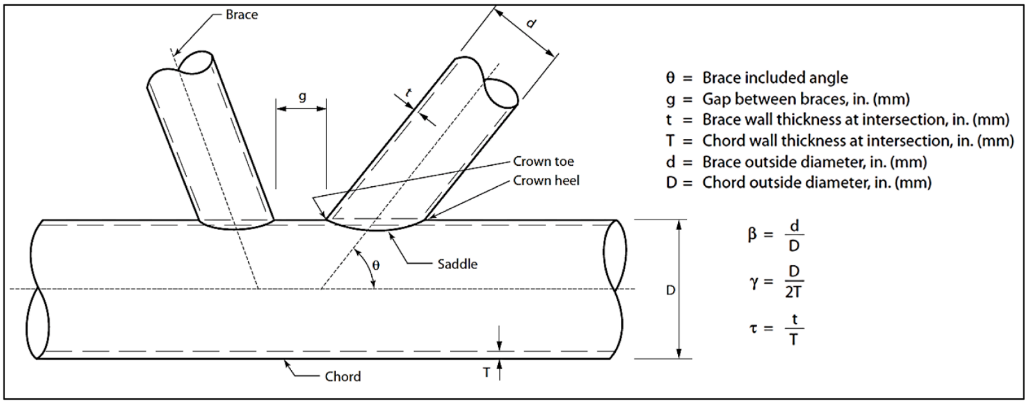

Fig. 3. Geometric parameters of offshore tubular joints [30].

assumption of rigid connections can show noticeable differences from the actual behavior of the structure. These differences can change some aspects, such as structural deformations, internal force distributions, and the structure's natural frequencies, especially in three-dimensional structures. Therefore, accounting for the effects of connection flexibility in the overall structural analysis is of utmost importance.

Researchers have focused on the significance of considering connection flexibility. Studies and experiments have been conducted on tubular connections, and their results can generally be categorized as empirical formulas and relationships derived from experiments and methods for modeling connections in a manner that accounts for flexibility. **Computational Models include** finite element models and analytical approaches that treat the joint as a separate structural component with defined stiffness properties. Computational models are more precise but require significant computational effort. **Empirical Formulations** are derived from experimental observations and provide direct equations for estimating joint flexibility. They are widely used in design codes and offer simplified expressions based on test data.

The earliest empirical model for local joint flexibility (LJF) was proposed by DNV (Det Norske Veritas). This model provides equations for rotational stiffness in T-joints under in-plane and out-of-plane bending. Fessler et al. expanded upon the DNV research to simulate the behavior of tubular joints under axial and bending loads. Efthymiou utilized finite element analysis to model tubular joints and developed empirical formulations for different joint types (T, Y, and K joints). Ueda et al. extended the study of joint flexibility by analyzing both elastic and plastic deformations and emphasized the nonlinear effects of joint deformation, which were crucial for offshore engineering applications.

The MSL Engineering Corporation develops relationships to calculate the capacity of tubular connections in fixed offshore structures. These relationships were obtained by studying a large number of different connections using the finite element method. They collected and studied all the samples and numerical data obtained from the load-bearing behavior of tubular connections, and by utilizing this data, they were able to propose relationships that result in force-displacement and moment-rotation diagrams for any connection, both in the linear and non-linear regions. Among the advantages and factors considered in the proposed formulas, which were not present in previous studies, are considering the interaction of the base section of the connection, classification of axial loads on the connection, interaction between force-displacement and moment-rotation diagrams (P-δ and M-θ), limitations related to toughness and brittleness and consideration of load-bearing behavior s. MSL provided the capacity relationships for the connections in the three states. The mean ultimate represents the statistical mean failure load of the joints tested, corresponding to the peak of the force-displacement curve or the "most probable failure load.". Characteristic ultimate is based on the same data as the mean ultimate capacity; however, this value is reduced to account for the variability in test results, providing a conservative estimate of the joint's capacity. The characteristic first crack, which in most cases, equals the characteristic ultimate capacity but is further reduced to prevent joint degradation under repeated loading. This capacity is recommended for structures subjected to cyclic loads, such as wave loading. The MSL suggested Eq. (16) and Eq. (17) to calculate the axial and bending strength of the tubular joints.

$$N_{Rd} = \frac{f_y T^2}{\sin\theta} Q_u Q_f \tag{16}$$

$$N_{Rd} = \frac{f_y T^2 d}{\sin\theta} Q_u Q_f \tag{17}$$

Where f_y is the yield strength of chord material, T is the chord thickness, θ is the brace angle, Q_u is the joint strength factor, and Q_f is the chord stress factor.

In these formulas, the Q_u calculates based on the shape of the joint, the loading state, and the loading configuration, depending on other factors such as shape factor (Q_β), distance factor (Q_g), and angle correction ratio (Q_{yy}). Also, Q_f can be calculated using Eq. (18), where λ is a coefficient that depends on the joint's geometry and loading conditions, and U is the chord stress utilization factor, representing the ratio of the applied stress in the chord to the yield strength of the chord material.

$$Q_f = 1 - \lambda U^2 \tag{18}$$

In this paper, the SAP2000 software version 21 was utilized to analyze the platform under applied environmental loads. Additionally, to account for the flexibility of connections, in section A.14.2.2 of the ISO 19902 standard for the design of fixed steel jackets, the use of MSL relationships is considered both the linear and nonlinear aspects of connections. In this study, a secondary connection to the main member was considered using a weightless intermediate member to model the flexibility of joints. The length of these elements is equal to the radius of the primary member. The corresponding force-displacement and bending-rotation diagrams, which were obtained using the relationships provided by MSL for axial compression and tension loading as well as in-plane and out-of-plane bending loading based on the geometry and specifications of the connection, were applied to these elements during the optimization process. In Fig. 4, a schematic diagram of rigid and flexible connections in a K-shape joint is shown.

4. Results

Table 6 summarises the optimization process results of different scenarios; Fig. 5 shows the trend of convergence during the optimization process. Based on the results, Model-1 achieved a weight reduction to 996 tons (31% optimization degree) after completing 93 generations. At

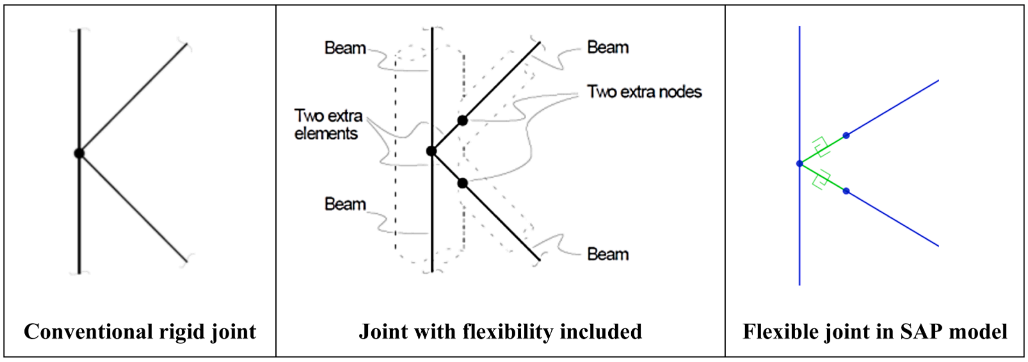

Fig. 4. The schematic diagram of rigid and flexible connections in a K-shape joint.

Table 6
The summary of the results of the optimization process based on the scenario.

Characteristics	Model-1		Model-2		Model-3		Model-4	
	Initial	Optimized	Initial	Optimized	Initial	Optimized	Initial	Optimized
Structural period (Sec)	1.02	1.15 (+13%)	1.56	1.83 (+17%)	1.60	1.91 (+19%)	1.56	1.67 (+7%)
Reference point deflection (mm)	65.7	81.2 (+24%)	103.4	147.0 (+42%)	110.5	156.4 (+41%)	103.4	125.5 (+21%)
δ_h/H	0.0010	0.0013	0.0016	0.0023	0.0017	0.0024	0.0016	0.0019
Total weight (ton)	1437	996	1437	943	1437	934	1437	1170
Optimization degree	31%		34%		35%		19%	
FEA time (s/run)	2400 ± 150		2650 ± 210		2700 ± 180		1800 ± 120	
GA time (s/run)	180 ± 15		190 ± 20		200 ± 18		150 ± 10	
Total runtime (s)	2580 ± 160		2840 ± 220		2900 ± 200		1950 ± 130	
Generations	93		97		100		66	

this point, the optimization process was terminated. The structural period increased from 1.02 to 1.15 sec, and the reference point deflection rose from 65.7 mm to 81.2 mm. This indicates that while weight reduction was significant, the structural stiffness decreased, leading to higher deformations.

Model-2 demonstrated a more significant improvement, with a weight reduction to 943 tons (34% optimization degree) over 97 generations. By incorporating flexible connections into the platform modeling, the structure exhibited better load distribution, reduced stress concentrations, and enhanced optimization compared to Model-1. The increased structural period (1.83 sec) and deflection (147.0 mm) reflect the influence of joint flexibility, which aligns more closely with the real-world elastic-plastic behavior of tubular connections.

Model-3 achieved the highest optimization degree of 35% (934 tons) after 100 generations. The use of API connection capacity criteria within nonlinear MSL relations introduced slightly greater flexibility compared to Model-2, as seen in the marginal increases in structural period (1.91 sec) and deflection (156.4 mm). This suggests that refining connection modelling criteria can enhance optimization outcomes.

Model-4 showed limited success, with only a 19% optimization degree (1170 tons) after 66 generations. The fixed geometry of diagonal and horizontal braces restricted load redistribution, forcing jacket legs (e.g., LG-2 and LG-3 with 42% and 36% participation rates) to bear higher loads. Despite significant sectional reductions in jacket legs (e.g., LG-2: 175.5×6.5 mm → 167.5×2.5 mm), the rigidity of other members limited overall weight savings.

A critical observation from the results is the superiority of flexible connection models (Models 2 and 3) over rigid-joint assumptions (Model-1). Traditional rigid-joint analyses neglect localised deformations at tubular connections, leading to conservative designs with excessive material use. In reality, connections exhibit elastic-plastic behavior under load, redistributing stresses and allowing for thinner sections. For example, in Model-2, horizontal braces (HB-1) were reduced from 66×2.54 mm to 59.73×1.905 mm without compromising structural integrity, contributing to the 34% weight reduction. The comparison between Models 2 and 3 highlights the nuanced role of connection capacity criteria. While both models assumed flexible joints, Model-3's use of API-derived capacities introduced minor additional flexibility, enabling a 1% higher optimization degree. This underscores the importance of adopting industry standards like API to better capture nonlinear material behavior and failure modes.

Table 6 also summarizes runtimes. Flexible-joint models required approximately 10–15% longer FEA time due to added joint elements, while GA overhead remained a minor fraction (<8%) of total runtime. Total runtimes per optimization run ranged between 20 and 60 minutes on a standard workstation (Intel i7, 32 GB RAM).

The convergence trends in Fig. 5 further validate the results. Models 1–3 exhibited steady progress over 90–100 generations, reflecting a robust exploration of the design space. In contrast, Model-4 stagnated after 66 generations due to constraints on brace geometry, which limited variable adjustments. This premature termination highlights the necessity of flexible design parameters to achieve full optimization potential. Since genetic algorithms are stochastic, each optimization scenario was repeated 20 times with different random seeds. The reported results represent the mean values, and error bars (standard deviations) to illustrate the variability of outcomes. As can be seen in graphs, in the initial steps, the models show a high coefficient of variation (in the range of 5% to 13%); however, it reduced with optimization progress.

Fig. 5 also shows violation histories. Models 1–3 converge to feasible populations by generations 70–100 (fraction feasible >85%). Model-4 retained significant punching-shear violations and reached only 55% feasible individuals at termination, consistent with its limited weight reduction. During early generations, maximum violations reached values B_n=1.6–1.4, but the dynamic penalty rapidly reduced to below 1.2. By convergence, the best individuals satisfied all constraints with final violation ratios $B_n \leq 1.0$ (within numerical tolerance).

Table 7 reveals that jacket legs (LG groups) played a pivotal role in optimization, particularly in Model-4. For instance, LG-2 achieved a 42% participation rate after reducing its thickness from 6.5 mm to 2.5 mm. However, the fixed geometry of braces in Model-4 created a

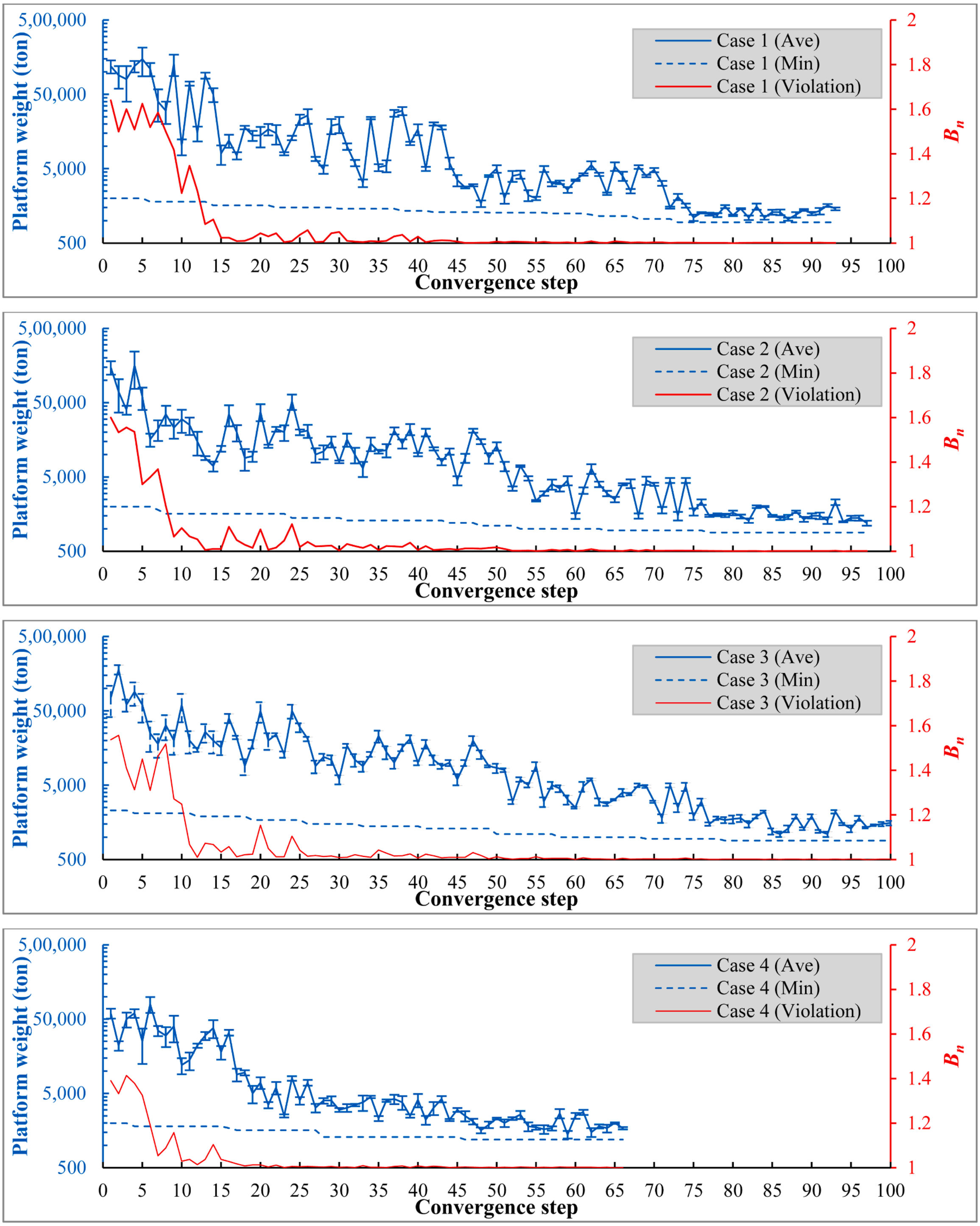

Fig. 5. The trend of convergence during the optimization process based on the scenario.

bottleneck: forces concentrated on jacket legs could not be offset by optimizing horizontal/vertical braces (HB/VB), which retained their original sections (e.g., HB-1 remained at 66×2.54 mm). This contrasts sharply with Models 2–3, where braces were actively optimized (e.g., VB-3: 61×3.81 mm to 50.8×1.588 mm), enabling holistic weight reduction.

Finally, the review of stress values shows that the UC values (**Unity Check**, defined as the ratio of the actual stress in a member to its corresponding allowable stress) in all cases were below one, indicating that the optimized designs satisfied the API RP 2A allowable stress requirements and thus remained structurally safe. In Fig. 6, the UC distributions for Model-1 and Model-4 are presented. It is noted that in Model-4 only the jacket legs were optimized, while the brace members retained their initial sections, which resulted in noticeable reductions of UC values in the legs but little improvement in the braces. This selective optimization explains the lower overall efficiency of Model-4 compared with the fully optimized models..

6. Conclusion

This study developed a genetic algorithm framework to optimize offshore jacket platforms by integrating joint flexibility. The goal was to

Table 7
Details of initial and optimized tubular section sizes due to the optimization process.

Model and groups		Initial Design		Optimized Design		
		Member Section (Cm)	Pile Section (Cm)	Member Section (Cm)	Pile Section (Cm)	Participation in optimization
Model-1	HB-1	66×2.54	-	59.73×1.905	-	8%
	HB-2	66×2.54	-	59.73×1.905	-	6%
	HB-3	61×2.54	-	50.8×2.54	-	2%
	HB-4	61×2.54	-	45.7×1.27	-	6%
	VB-1	86.4×2.54	-	66×2.54	-	7%
	VB-2	61×2.54	-	59.73×1.905	-	4%
	VB-3	61×3.81	-	59.73×1.905	-	9%
	LG-1	175.5×6.5	152.4×4.445	171.23×4.365	152.4×4.445	16%
	LG-2	175.5×6.5	152.4×4.445	167.5×2.5	152.4×4.445	21%
	LG-3	175.5×6.5	152.4×4.445	166.5×2	152.4×4.445	20%
Model-2	HB-1	66×2.54	-	59.73×1.905	-	8%
	HB-2	66×2.54	-	50.8×2.54	-	4%
	HB-3	61×2.54	-	50.8×1.588	-	6%
	HB-4	61×2.54	-	45.7×1.27	-	5%
	VB-1	86.4×2.54	-	61×2.54	-	9%
	VB-2	61×2.54	-	50.8×2.54	-	3%
	VB-3	61×3.81	-	50.8×1.905	-	10%
	LG-1	175.5×6.5	152.4×4.445	171.23×4.365	152.4×4.445	14%
	LG-2	175.5×6.5	152.4×4.445	166.5×2	152.4×4.445	21%
	LG-3	175.5×6.5	152.4×4.445	166.5×2	152.4×4.445	18%
Model-3	HB-1	66×2.54	-	59.73×1.905	-	8%
	HB-2	66×2.54	-	50.8×2.54	-	4%
	HB-3	61×2.54	-	50.8×1.588	-	6%
	HB-4	61×2.54	-	45.7×1.27	-	5%
	VB-1	86.4×2.54	-	61×2.54	-	9%
	VB-2	61×2.54	-	50.8×2.54	-	3%
	VB-3	61×3.81	-	50.8×1.588	-	11%
	LG-1	175.5×6.5	152.4×4.445	171.23×4.365	152.4×4.445	14%
	LG-2	175.5×6.5	152.4×4.445	166.5×2	152.4×4.445	21%
	LG-3	175.5×6.5	152.4×4.445	166.5×2	152.4×4.445	18%
Model-4	HB-1	66×2.54	-	66×2.54	-	-
	HB-2	66×2.54	-	66×2.54	-	-
	HB-3	61×2.54	-	61×2.54	-	-
	HB-4	61×2.54	-	61×2.54	-	-
	VB-1	86.4×2.54	-	86.4×2.54	-	-
	VB-2	61×2.54	-	61×2.54	-	-
	VB-3	61×3.81	-	61×3.81	-	-
	LG-1	175.5×6.5	152.4×4.445	172.5×5	152.4×4.445	22%
	LG-2	175.5×6.5	152.4×4.445	167.5×2.5	152.4×4.445	42%
	LG-3	175.5×6.5	152.4×4.445	167.5×2.5	152.4×4.445	36%

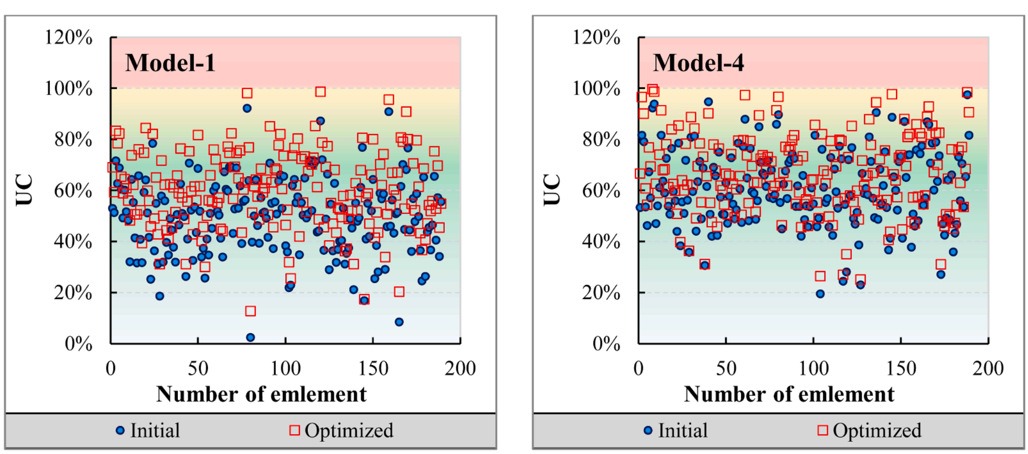

Fig. 6. The UC values calculated before and after optimization.

balance structural integrity, material efficiency, and cost, addressing gaps in traditional rigid-joint models and advancing sustainable design practices for dynamic marine environments. From the results, the following conclusions can be drawn:

- Model-1 (rigid joints) achieved a 31% weight reduction (996 tons) but exhibited reduced stiffness, with the structural period rising from 1.02 to 1.15 sec and deflection from 65.7 to 81.2 mm. This highlights the conservatism inherent in rigid joint models, which underestimate real-world joint deformations.
- Models incorporating flexible connections (Model-2 and Model-3) outperformed traditional rigid-joint assumptions (Model-1). Model-2 achieved a 34% weight reduction (from 1,437 to 943 tons) with an increased structural period (1.83 sec) and reference point

deflection (147.0 mm), reflecting stress redistribution through elastic-plastic joint behavior. Model-3, which integrated API RP 2A joint capacity criteria, further improved optimization to 35% (934 tons), underscoring the value of codified nonlinear material behavior in design.

- The genetic algorithm exhibited robust convergence over 90–100 generations for Models 1–3. Model-4 stagnated prematurely (66 generations), emphasizing the need for flexible design parameters to explore the solution space effectively.
- Jacket legs dominated optimization efforts, particularly in Model-4, where LG-2 participation reached 42% after sectional reductions. However, fixed braces in Model-4 restricted overall efficiency, yielding only 19% optimization (1,170 tons) due to retained original brace sections. In contrast, Models 2–3 achieved holistic savings by optimizing braces.
- While the study showed improvements in weight reduction and realistic structural response, several limitations should be acknowledged. The study focuses on jacket geometry and specific loading conditions and should be extended to other offshore structures to broaden its scope and applicability. Joint flexibility is modeled using MSL and API RP 2A formulations, which, although widely accepted, may not represent the full range of possible nonlinear joint behaviors or fabrication tolerances. The optimizations rely on a predefined library of 95 tubular sections. Fatigue performance, corrosion progression, and soil–structure interaction effects were not included in the optimization and should be addressed in future work.

CRediT authorship contribution statement

Naser Shabakhty: Writing – review & editing, Writing – original draft, Supervision, Project administration, Methodology, Investigation, Conceptualization. **Hamid Reza Karimi:** Writing – review & editing, Writing – original draft, Visualization, Software, Methodology, Investigation, Formal analysis, Data curation, Conceptualization. **Abbas Yeganeh-Bakhtiay:** Writing – original draft, Supervision, Resources, Project administration, Formal analysis, Data curation. **Mohammad Ghanbarian:** Writing – original draft, Software, Resources, Investigation, Formal analysis, Data curation.

Declaration of competing interest

The authors declare that they have no known competing financial interests or personal relationships that could have appeared to influence the work reported in this paper.

Data availability

Data will be made available on request.

References

[1] M. Hezarjaribi, M.R. Bahaari, V. Bagheri, H. Ebrahimian, Sensitivity analysis of jacket-type offshore platforms under extreme waves, J. Constr. Steel. Res. 83 (2013) 147–155, https://doi.org/10.1016/j.jcsr.2013.01.013.
[2] N. Shabakhty, E. Jabbari, J. Salehi, Reliability analysis of damaged jacket platform under ship impact, Mar.-Eng. 14 (2018) 111–117.
[3] N. Shabakhty, A. Khansari, Fatigue analysis of a jacket structure to linear and weakly nonlinear random waves, J. Offshore Mech. Arct. Eng. 141 (2019), https://doi.org/10.1115/1.4042946.
[4] A. Mojtahedi, H. Hokmabady, A. Yaghubzadeh, S. Mohammadyzadeh, An improved model reduction-modal based method for model updating and health monitoring of an offshore jacket-type platform, Ocean Eng. 209 (2020) 107495, https://doi.org/10.1016/j.oceaneng.2020.107495.
[5] T. Nasseri, N. Shabakhty, M.H. Afshar, Study of fixed jacket offshore platform in the optimization design process under environmental loads, IJMT 2 (2014) 75–84. http://ijmt.ir/article-1-289-en.html.
[6] H.R. Karimi, N.S. Karamzadeh, E.O. Rabei Gholami, Assessing the behavior of fixed offshore jackets in failure condition, evaluation in ultimate State to improve structural safety, Eng. Rep. 7 (2025) e70179, https://doi.org/10.1002/eng2.70179.
[7] H.R. Karimi, N. Shabakhty, A comparative assessment of the impact of tilting on structural safety and behavior of fixed offshore platforms, Appl. Ocean Res. 136 (2023) 103589, https://doi.org/10.1016/j.apor.2023.103589.
[8] H.R. Karimi, N.S. KaramZadeh, E.O.R. Golami, Effect of elevational and member damage on jacket strength: sensitivity and reliability review of South Pars phase-20 jacket, using push-over analysis, Ocean Eng. 143 (2017) 209–216, https://doi.org/10.1016/j.oceaneng.2017.08.001.
[9] H. Moradi, H.R. Karimi, N.S. KaramZadeh, E. O'Din Rabei Golami, Effects of leg slope on the failure of fixed jacket platforms: A case study of south pars gas Field's platforms, Ocean Eng. 210 (2020) 107401, https://doi.org/10.1016/j.oceaneng.2020.107401.
[10] P. Rezadoost, B. Asgarian, H. Nassiraei, Degree of bending of FRP-reinforced tubular X-joints in offshore jacket-type structures under in-plane bending moment, Ocean Eng. 307 (2024) 118114, https://doi.org/10.1016/j.oceaneng.2024.118114.
[11] A.R. Damanpack, A new finite joint element to model joint connections in offshore structures, Mar. Struct. 103 (2025) 103797, https://doi.org/10.1016/j.marstruc.2025.103797.
[12] H. Ahmadi, V. Mayeli, Probabilistic analysis of the local joint flexibility in two-planar tubular DK-joints of offshore jacket structures under in-plane bending loads, Appl. Ocean Res. 81 (2018) 126–140, https://doi.org/10.1016/j.apor.2018.10.011.
[13] N. Shabakhty, H.R. Karimi, A. Yeganeh-Bakhtiary, M. Ghanbarian, Structural optimization of offshore jacket platforms considering structure-pile-soil interactions, using a continuous genetic algorithm, Appl. Ocean Res. 164 (2025) 104767, https://doi.org/10.1016/j.apor.2025.104767.
[14] A.A. Motlagh, N. Shabakhty, A. Kaveh, Design optimization of jacket offshore platform considering fatigue damage using genetic algorithm, Ocean Eng. 227 (2021) 108869, https://doi.org/10.1016/j.oceaneng.2021.108869.
[15] L. Zhou, P. Huang, S. Chi, M. Li, H. Zhou, H. Yu, H. Cao, K. Chen, Structural health monitoring of offshore wind power structures based on genetic algorithm optimization and uncertain analytic hierarchy process, Ocean Eng. 218 (2020) 108201.
[16] M. Ghasri, H.R. Karimi, A. Salarnia, A metaheuristic optimization framework inspired by virus mutations and its ability to optimize the structural design of 2D and 3D steel frames compared to other methods, Results. Eng. 26 (2025) 105020, https://doi.org/10.1016/j.rineng.2025.105020.
[17] V. Aghaeidoost, S. Afshar, N. Ziaie Tajaddod, B. Asgarian, H.R Shokrgozar, Damage detection in jacket-type offshore platforms via generalized flexibility matrix and optimal genetic algorithm (GFM-OGA), Ocean Eng. 281 (2023) 114841, https://doi.org/10.1016/j.oceaneng.2023.114841.
[18] X. Wen, G. Yin, T. Liu, M.C. Ong, C. Wang, K. Wang, An optimization framework for mooring design of floating offshore wind turbines using a genetic algorithm based on a surrogate model, Renew. Energy (2025) 122807, https://doi.org/10.1016/j.renene.2025.122807.
[19] L. Yang, B. Li, K. Zhang, C. Huang, F. Jing, Multi-objective shape optimization of offshore swirl-vane oil-water separators using genetic algorithm network coupled computational fluid dynamics, Ocean Eng. 325 (2025) 120827, https://doi.org/10.1016/j.oceaneng.2025.120827.
[20] X. Zhang, Q. Wang, S. Ye, K. Luo, J. Fan, Efficient layout optimization of offshore wind farm based on load surrogate model and genetic algorithm, Energy 309 (2024) 133106, https://doi.org/10.1016/j.energy.2024.133106.
[21] T. Gentils, L. Wang, A. Kolios, Integrated structural optimisation of offshore wind turbine support structures based on finite element analysis and genetic algorithm, Appl. Energy 199 (2017) 187–204, https://doi.org/10.1016/j.apenergy.2017.05.009.
[22] B. Benítez-Suárez, R. Quevedo-Reina, G.M. Álamo, L.A. Padrón, PSO-based design and optimization of jacket substructures for offshore wind turbines, Mar. Struct. 101 (2025) 103759, https://doi.org/10.1016/j.marstruc.2024.103759.
[23] R.O. Ivanhoe, L. Wang, A. Kolios, Generic framework for reliability assessment of offshore wind turbine jacket support structures under stochastic and time dependent variables, Ocean Eng. 216 (2020) 107691, https://doi.org/10.1016/j.oceaneng.2020.107691.
[24] Y.-S. Lee, J.A. González, J.H. Lee, Y. Il Kim, K.C. Park, S. Han, Structural topology optimization of the transition piece for an offshore wind turbine with jacket foundation, Renew. Energy 85 (2016) 1214–1225, https://doi.org/10.1016/j.renene.2015.07.052.
[25] Z. Wang, S.K. Mantey, X. Zhang, A numerical tool for efficient analysis and optimization of offshore wind turbine jacket substructure considering realistic boundary and loading conditions, Mar. Struct. 95 (2024) 103605, https://doi.org/10.1016/j.marstruc.2024.103605.
[26] A.E. Eiben, J.E. Smith, Introduction to Evolutionary Computing, Springer, Berlin Heidelberg, 2013.
[27] R. Chelouah, P. Siarry, A continuous genetic algorithm designed for the global optimization of multimodal functions, J. Heuristics 6 (2000) 191–213, https://doi.org/10.1023/A:1009626110229.
[28] K.F. Man, K.S. Tang, S. Kwong, Genetic Algorithms: Concepts and Designs, Springer, London, 2012.
[29] O. Kramer, Genetic Algorithm Essentials, Springer International Publishing, 2017.
[30] Recommended practice for planning, designing, and constructing fixed offshore platforms: working stress design, American Petroleum Institute, 2005.